JACS
JOURNAL OF THE AMERICAN CHEMICAL SOCIETY
Article
pubs.acs.org/JACS

Photoluminescence Brightening via Electrochemical Trap Passivation in ZnSe and Mn^{2+}-Doped ZnSe Quantum Dots

Amanda L. Weaver and Daniel R. Gamelin*

Department of Chemistry, University of Washington, Seattle, Washington 98195-1700, United States

Supporting Information

ABSTRACT: Spectroelectrochemical experiments on wide-gap semiconductor nanocrystals (ZnSe and Mn^{2+}-doped ZnSe) have allowed the influence of trap electrochemistry on nanocrystal photoluminescence to be examined in the absence of semiconductor band filling. Large photoluminescence electrobrightening is observed in both materials upon application of a reducing potential and is reversed upon return to the equilibrium potential. Electrobrightening is correlated with the transfer of electrons into nanocrystal films, implicating reductive passivation of midgap surface electron traps. Analysis indicates that the electrobrightening magnitude is determined by competition between electron trapping and photoluminescence (ZnSe) or energy transfer (Mn^{2+}-doped ZnSe) dynamics within the excitonic excited state, and that electron trapping is extremely fast ($k_{trap} \approx 10^{11}$ s^{-1}). These results shed new light on the complex surface chemistries of semiconductor nanocrystals.

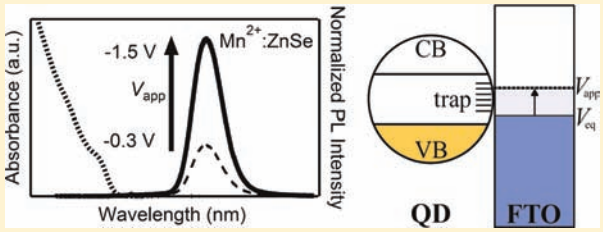

INTRODUCTION

The photoluminescence (PL) of colloidal semiconductor nanocrystals (or quantum dots, QDs) is strongly influenced by surface chemistry. Surface states within the semiconductor optical gap may introduce effective nonradiative decay pathways that reduce PL quantum yields.[1−6] In some cases, surface traps can be passivated by judicious selection of capping ligands[2,7,8] or by growth of conformal inorganic shell layers,[9−15] increasing PL quantum yields. Trap passivation can even occur photochemically ("photobrightening"),[16−18] which has been proposed to involve photoinduced annealing,[19−21] photooxidation or reduction,[22] ligand chemistry,[23] photoinduced adsorption of small molecules,[24−26] or photoelectrification.[27−29] Photobrightening is influenced by reducing agents,[30] and in nanowires it has been enhanced by low levels of electron injection using an AFM tip.[31] Collectively, these data provide circumstantial evidence that QD PL may be manipulated by controlling the charge states of surface traps. Spectroelectrochemical studies of the relationship between surface-trap redox chemistry and QD PL are needed to test the validity of this hypothesis.

Previous spectroelectrochemical studies of colloidal QDs have focused primarily on charge injection into quantum-confined band levels of easily reduced QDs with relatively positive conduction-band (CB) potentials (e.g., CdSe, CdS, ZnO, PbSe).[32−52] It is now established that electron injection into the CBs of colloidal chalcogenide QDs bleaches the first excitonic absorption ($1S_h \rightarrow 1S_e$), introduces new absorption due to intra-conduction-band ($1S_e \rightarrow 1P_e$) electronic excitation, and substantially diminishes excitonic PL quantum yields through electron-exciton Auger recombination.[33−36,38,40−48] To date, however, there have been no reports of the spectroelectrochemistry of semiconductor nanocrystals with very negative CB potentials, for which CB filling is deliberately avoided (e.g., ZnSe, ZnS). In such QDs, midgap surface states are exposed and readily accessible to electrochemical manipulation, making them particularly attractive for investigation of the influence of surface redox chemistry on nanocrystal photophysics.

Here, we describe the spectroelectrochemistry of ZnSe QDs. A remarkably large (~40-fold) enhancement of steady-state PL is observed when ZnSe QDs are held under a cathodic bias. In agreement with recent blinking results,[51] this electrobrightening implicates elimination of a fast nonradiative channel for exciton deactivation via reductive surface electron-trap passivation. Incorporation of Mn^{2+} dopants into the ZnSe QDs introduces a well-defined fast exciton-deactivation pathway that allows the electron trap kinetics to be clocked. Analysis of the difference in PL electrobrightening magnitudes with and without Mn^{2+} yields an effective electron trapping rate constant of ~10^{11} s^{-1}, comparable to that for energy transfer to Mn^{2+}, and much greater than that for excitonic PL. These findings provide new insight into the roles of surface trap states on QD photoluminescence.

EXPERIMENTAL SECTION

Colloidal ZnSe and Mn^{2+}:ZnSe QDs were synthesized and characterized as detailed previously.[53,54] QDs made by cluster thermolysis[53] and hot-injection[54] routes gave essentially identical results. QD films were prepared by depositing QD suspensions in toluene onto a 3-mercaptopropyl-trimethoxysilane treated fluorine doped tin oxide (FTO) surface, cross-linking the QDs with 1,7-

Received: February 2, 2012
Published: March 14, 2012

   dx.doi.org/10.1021/ja301102h | J. Am. Chem. Soc. 2012, 134, 6819−6825

heptanediamine, and curing under vacuum at 70 °C for 1 h.[42,45,47] Absorption measurements were performed using a Cary 500 (Varian) spectrometer. Continuous-wave PL spectra were collected using either 363 nm excitation and a 0.5 m monochromator and CCD for detection, or 405 nm excitation and an Ocean Optics USB2000 spectrometer for detection. Time-resolved PL measurements were performed with excitation at 360 nm and PMT detection at 590 nm (25 nm spectral band-pass). Electrobrightening was independent of excitation wavelength. Photoluminescence quantum yields were measured on QD films using an integrating sphere and were assumed to be the same in the electrochemical cell at the equilibrium potential.

The electrochemical cells consisted of silver pseudo-reference electrodes, platinum counter electrodes, and films of QDs on FTO as the working electrodes. The cells were assembled under N_2 atmosphere, with 0.1 M tetrabutylammonium perchlorate (TBAP) in dimethylformamide (DMF) as the electrolyte. The electrochemical experiments were conducted using a μ-autolab II potentiostat. All measurements were performed at room temperature in cuvettes sealed under anaerobic atmosphere. Care was taken to avoid illumination of the Ag^0 electrode. For estimation of the number of electrons added per QD, the number of QDs per unit area in a given film was estimated by absorption spectroscopy using an empirical ZnSe QD molar extinction coefficient of 4.6×10^5 $M^{-1}cm^{-1}$,[55] and the total number of electrons added to a QD film was estimated by integrating the time-resolved current obtained during a potential-step experiment after subtracting a baseline determined by the steady-state current at the applied potential.[32]

As observed previously,[50,56] the equilibrium potentials of these QD films drifted over the course of many hours, and differed for measurements performed on the same films on different days, or on different films of the same QDs. The drifting equilibrium potentials likely reflect the use of Ag^0 pseudo-reference electrodes. With the exception of such variations in equilibrium potential, however, all measurements yielded very similar results. Over 25 different films from four different QD syntheses were examined, and all showed essentially the same electrobrightening as reported here. The electrobrightening results are therefore always reported together with PL measured at or near the equilibrium potential. Within a given experiment, this drift was negligible and the electrobrightening was stable, reversible, and reproducible, as illustrated by the data reported here.

RESULTS AND ANALYSIS

Electrobrightening. Figure 1a illustrates the electrochemical cells used to introduce charge carriers into ZnSe QD films. Starting at the equilibrium potential (V_{eq}), a cathodic bias was applied (V_{app}) while monitoring the QD PL. The ZnSe QD CB potentials are very negative (~ −2.0 V vs Ag^0), allowing selective reduction of midgap traps without injection of electrons into the CB.

Figure 1b plots absorption and PL spectra of a ZnSe QD film at the equilibrium potential (V_{eq} = −0.2 V) and after electrobrightening at V_{app} = −1.5 V. The absorption spectrum of the colloidal ZnSe QDs shows the first excitonic maximum at ~385 nm, consistent with $d \approx 3.2$ nm nanocrystals. The PL spectrum of the same QDs in a film on FTO shows a weak excitonic feature at ~415 nm and broad trap emission centered at ~500 nm. Application of a cathodic bias leads to electron transfer into the QD film and increases the total PL quantum yield (including both excitonic and trap PL) from $\Phi \approx 0.7\%$ to $\Phi \approx 11\%$. The excitonic PL intensity at 385 nm changes by $I_{EB}/I_0 \approx 40$. Trap PL at 500 nm also increases with applied potential, by $I^{tr}_{EB}/I^{tr}_0 \approx 10$. Both exciton and trap PL electrobrightening are completely reversed when the cell is returned to its equilibrium potential and the electrons are removed (vide infra). There is no discernible change in QD absorbance over this potential range. These observations are consistent with electrochemical passivation of surface electron traps.

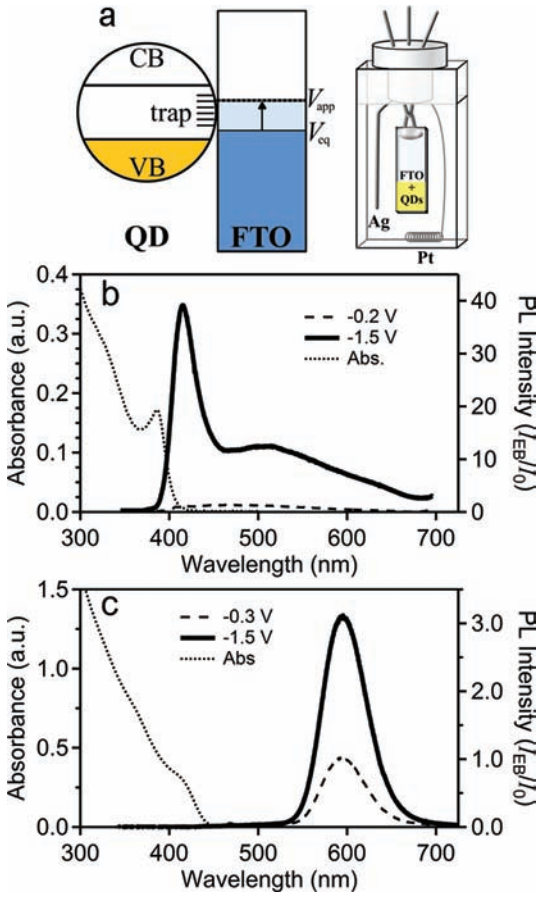

Figure 1. Spectroelectrochemistry of ZnSe QD films. (a) A schematic of an electrochemical cell (right) with a silver pseudo-reference electrode, platinum counter electrode, and a film of QDs on FTO as the working electrode. For V_{app} above the equilibrium potential of the working electrode, V_{eq}, midgap electron traps are filled (left). (b) The excitonic PL spectra at V_{eq} = −0.2 V (dashed) and after electrobrightening at V_{app} = −1.5 V (solid) vs Ag^0 for a ZnSe QD film. λ_{ex} = 363 nm. The absorption of the same ZnSe QDs as colloids is shown as a dotted line. (c) The Mn^{2+} PL spectra at the equilibrium potential of V_{eq} = −0.3 V (dashed), and after electrobrightening at V_{app} = −1.5 V (solid). λ_{ex} = 405 nm. The absorption of the colloidal Mn^{2+}:ZnSe QDs is shown as a dotted line.

An impurity can be used to create well-defined midgap electronic states that introduce new very fast nonradiative exciton deactivation channels. If fast electron trapping diminishes excitonic PL quantum yields as suggested by the above results, then less PL electrobrightening should be observed in Mn^{2+}-doped ZnSe QDs, where nonradiative exciton-to-Mn^{2+} energy transfer within a few tens of picosecond[57−60] competes with electron trapping, and the resulting luminescent Mn^{2+} $^4T_1$ excited state is not susceptible to electron trapping. To test this hypothesis, similar spectroelectrochemical measurements were performed on films of Mn^{2+}-doped ZnSe QDs (Mn^{2+}:ZnSe). Figure 1c plots absorption and PL spectra of Mn^{2+}:ZnSe QDs. The absorption spectrum of the colloidal QDs (dotted) shows the first excitonic feature at ~412 nm, consistent with $d \approx 5.0$ nm nanocrystals. At the equilibrium potential (V_{eq} = −0.3 V), the PL spectrum of the same QDs in a film on FTO (dashed) is dominated by the Mn^{2+} $^4T_1 \rightarrow {}^6A_1$ d−d transition centered at 595 nm,[61] with $\Phi \approx$

dx.doi.org/10.1021/ja301102h | J. Am. Chem. Soc. 2012, 134, 6819−6825

9.5%. Under cathodic bias (V_{app} = −1.5 V), electrons are transferred into the QD film and the Mn^{2+} PL quantum yield increases to $\Phi \approx 29.5\%$ (solid curve), that is, $I_{EB}^{Mn}/I_0^{Mn} \approx 3$. The Mn^{2+}:ZnSe QDs thus show an order of magnitude smaller PL electrobrightening than observed in comparable ZnSe QDs. From over 25 different films prepared from four different QD syntheses, $I_{EB}^{Mn}/I_0^{Mn} \approx 2.5 \pm 0.5$ and $I_{EB}/I_0 \approx 40 \pm 10$. We note that conduction band filling in Mn^{2+}-doped CdS QDs yields exceptionally efficient Mn^{2+} PL quenching,[50] opposite from the PL enhancement observed here. Also noteworthy is the fact that the $Mn^{2+/+}$ potential resides >1.5 eV above the ZnSe CB edge[62,63] and hence well outside the experimental potential window. These data thus support the interpretation that electrobrightening is linked to surface electron-trap passivation.

Figure 2a plots the Mn^{2+} PL intensity and the electrochemical current density measured simultaneously as a function

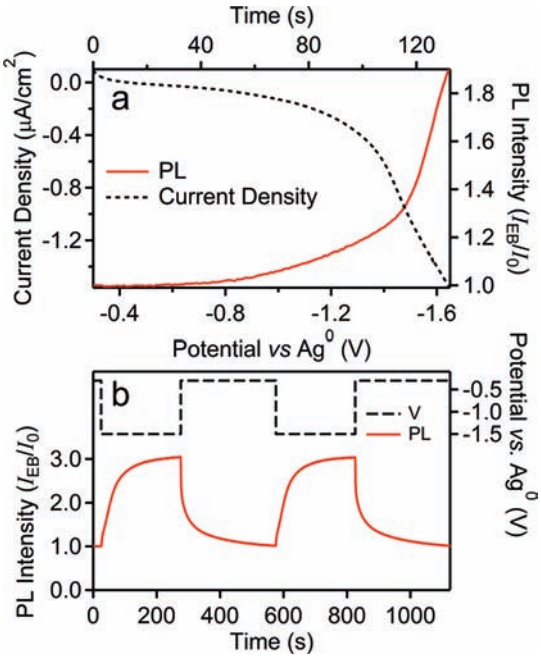

Figure 2. Electrobrightening of a Mn^{2+}:ZnSe QD film. (a) The current density (dashed) and the normalized PL intensity (solid) measured at 590 nm both increase as V_{app} is swept from −0.3 to −1.65 V at 0.01 V/s. (b) The normalized Mn^{2+} PL intensity (solid) and the applied potential vs Ag^0 (dashed) plotted versus time during a potential step experiment. λ_{ex} = 405 nm.

of applied potential (V_{app}) for the Mn^{2+}:ZnSe QDs. As V_{app} becomes more negative, both the current density and the PL intensity increase in concert. The onset potential for charging is ∼−0.8 V vs Ag^0, below the potentials at which conduction-band filling occurs in CdSe-based QDs (∼−1.0 V)[42] and CdS QDs (∼−1.3 V)[50] using similar electrochemical cells, and ∼1.2 V below the potential for ZnSe QD conduction-band filling (∼−2.0 V vs Ag^0) estimated from the bulk offset potentials of CdSe, CdS, and ZnSe.[64,65] This observation and the correlation between charging and PL strongly support the interpretation that electron trap reduction increases PL intensities. Figure 2b plots the PL intensity versus time for a measurement in which the potential was alternated between V_{eq} (−0.3 V) and V_{app} (−1.5 V), as indicated by the dashed line. The electrobrightening is reversible, and in both directions, the PL reaches steady state slowly after a few hundred seconds. These kinetics are attributed to slow diffusion of charge carriers through the QD film. Previous work has demonstrated extremely low electron mobilities in QD films at potentials below the CB edge potential,[41,44,66,67] consistent with the added electrons occupying localized QD surface states. Importantly, the electrobrightening of Figure 2b appears to be accompanied by transfer of *multiple* electrons/QD, not just one or fewer. From the experimental coulometry and the number of QDs on the working electrode, a value of >10 electrons/QD is estimated at $I_{EB}^{Mn}/I_0^{Mn} \approx 2.5$, albeit with sizable uncertainty (see Experimental Section). It is also interesting to note the inflections in both current density and PL at ∼−1.4 V, suggesting a rapidly changing trap density of states in that region.

Given that photoexcitation may itself induce PL brightening, it is necessary to address the dependence of this electrobrightening on photons. Figure 3 plots data intended to

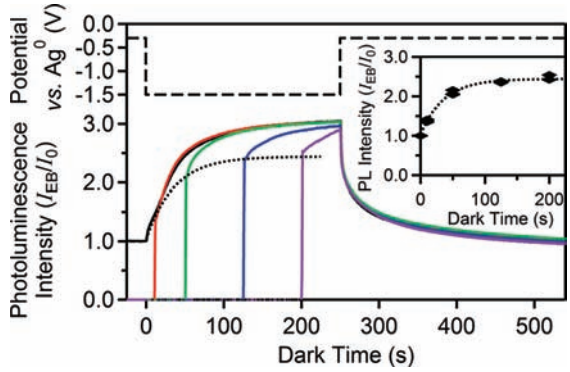

Figure 3. A cathodic bias (V_{app} = −1.5 V) is applied to a Mn^{2+}:ZnSe QD film for 250 s while the "dark time" is varied. The PL intensity at 590 nm versus time for dark periods of 0 s (black), 10 s (red), 50 s (green), 125 s (blue), and 200 s (purple), normalized at time = 0. An excitation power density of 150 mW/cm² (405 nm) was used. The dashed line represents the applied potential vs Ag^0 for all curves. Inset: The PL intensity at 590 nm measured within 1 s of photoexcitation, plotted versus dark time. The dotted curve shows a single-exponential fit to these data. This curve is reproduced in the main figure. λ_{ex} = 405 nm.

distinguish dark from photoinduced contributions to the electrobrightening shown in Figures 1 and 2. In these experiments, V_{app} = −1.5 V was applied at time = 0 with the QD film in the dark, and photons were turned on following a delay time ranging from 10 to 200 s. For comparison, the PL response obtained with continuous photoexcitation is also plotted. From these data, photoexcitation following application of a potential in the dark yields a large initial brightening followed by continued brightening on a much slower time scale. The magnitude of the initial brightening increases with increasing dark time (Figure 3, inset), converging to a value of ∼2.5 times the PL intensity at V_{eq} with an apparent time constant of $\tau_{eff} \approx 36$ s. Because this time constant reports on a dark process that occurs prior to photoexcitation, it is interpreted as reflecting slow electron diffusion through the QD film without assistance from photons, which may relate to spectral diffusion of reducible traps (see Discussion).

The data in Figure 3 also show slow additional brightening after photoexcitation is initiated. To probe the role of photons more thoroughly, the dependence of electrobrightening on photoexcitation power density was investigated. Figure 4a shows electrobrightening results for the sample from Figure 3,

dx.doi.org/10.1021/ja301102h | J. Am. Chem. Soc. 2012, 134, 6819−6825

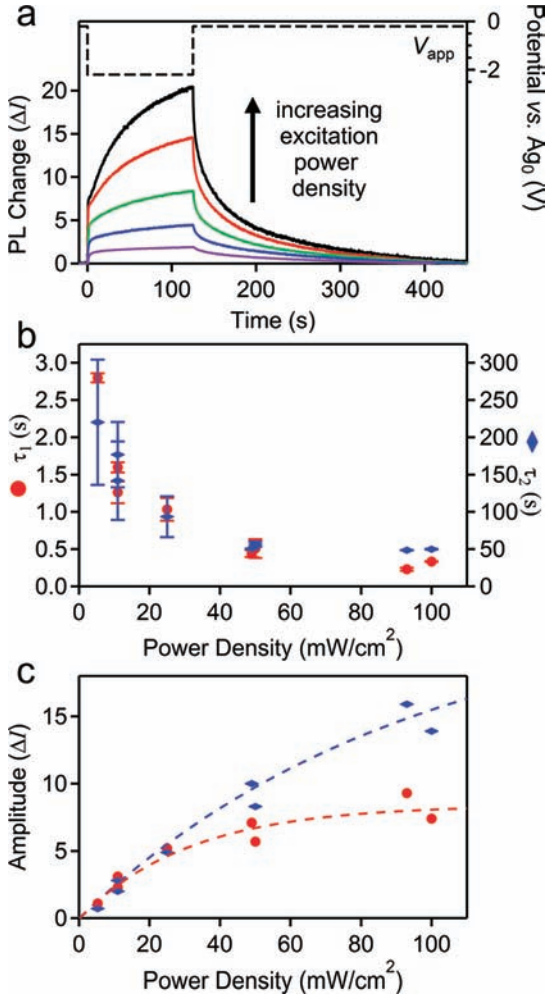

Figure 4. Dependence of PL electrobrightening on photoexcitation power density. (a) Change in Mn^{2+} PL intensity (ΔI) at 590 nm during electrobrightening measured at excitation power densities of 100, 50, 25, 11, and 5.3 mW/cm^2. The dashed line represents the cell potential vs Ag^0. (b) Time constants of the fast (τ_1) and slow (τ_2) contributions to the I_{EB}^{Mn} rise, plotted versus excitation power density. (c) Amplitudes of the fast (●) and slow (♦) components of the PL electrobrightening plotted versus excitation power density. The multiple data points represent results from independent measurements. The dashed curves are guides to the eye. λ_{ex} = 405 nm.

measured as a function of time at various photon power densities and plotted as $\Delta I = I_{EB} - I_0$, where I_0 is the PL intensity at V_{eq}. Overall, the trend in ΔI is largely due to the trend in excitation power, with more PL at higher powers as expected. At all excitation powers, ΔI increases quickly after V_{app} is stepped to reducing potentials, followed by a slower increase over the course of several minutes, and is describable using a double exponential function with apparent time constants τ_1 and τ_2 (see Supporting Information). Both time constants decrease with increasing photoexcitation power density (Figure 4b). Figure 4c plots the amplitudes of the fast and slow electrobrightening components versus photoexcitation power density. Both amplitudes increase with increasing power density as expected, but both also show saturation at high powers. From the QD extinction coefficient at the excitation wavelength, the highest experimental power density (100 mW/cm^2) corresponds to a per-QD excitation rate of only ~285 s^{-1}, below where Mn^{2+} saturation occurs.

The observation of two components in the electrobrightening (Figure 4b,c) may reflect inhomogeneity in the contact between the QDs and the FTO. For example, QDs in direct contact with the FTO may participate in rapid electron transfer and hence show fast electrobrightening, whereas QDs separated from the FTO by additional QD layers may show electrobrightening that is subject to slow electron percolation. The excitation power dependence is very complex, however. Although additional experiments would be necessary to fully unravel this power dependence, it is clear that both components are accelerated by photons (Figure 4b), consistent with observations of photoconductivity in QD solids.[68] Not only does photoexcitation improve electron mobility, but it also introduces a photobias that allows additional charging of the QD film, increasing electrobrightening. From comparison of the photoassisted and dark electrobrightening magnitudes in Figure 3, $V_{photobias} \approx -0.1$ to -0.4 V at 100 mW/cm^2 excitation.

Figure 5 shows semilog plots of Mn^{2+} PL decay data measured at V_{eq}, at V_{app}, and after return to V_{eq}. The inset plots

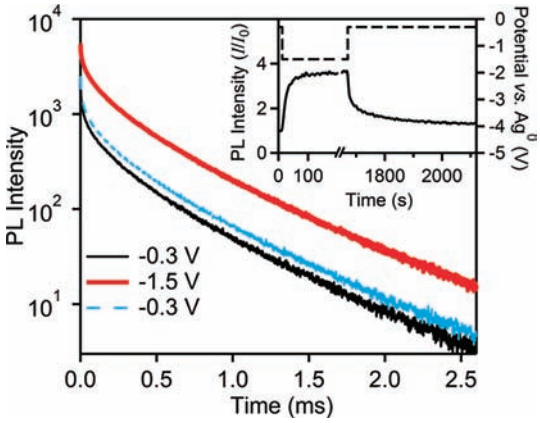

Figure 5. Mn^{2+} PL decay (590 nm) measured at various potentials for a film of Mn^{2+}:ZnSe QDs. The decay at V_{eq} = −0.3 V (black), V_{app} = −1.5 V (red, measured 190 s after V_{app}), and after the potential has been returned to V_{eq} = −0.3 V (blue, measured 480 s after return to V_{eq}). Inset: Mn^{2+} PL intensity at 590 nm (solid), normalized at 0 s. The dashed line represents the cell potential vs Ag^0. λ_{ex} = 360 nm.

the electrobrightening in a potential step experiment as in Figure 2b. Although these are different samples, it is noteworthy that the electrobrightening is essentially indistinguishable with 360 nm (Figure 5) and 405 nm (Figure 2) excitation. The Mn^{2+} PL decay dynamics in these three measurements are superimposable when normalized at ~2.0 ms (see the Supporting Information), indicating that the Mn^{2+} excited state is unaffected by the applied potential. Instead, the cathodic bias leads to *more* Mn^{2+} excitation. This result confirms that electrobrightening stems from elimination of exciton nonradiative decay pathways, which compete with the exciton-to-Mn^{2+} energy transfer. Exciton-to-Mn^{2+} energy transfer is extremely fast in these and related doped semiconductor nanocrystals, with typical rate constants of $k_{ET} \approx 10^{11}$ s^{-1},[57−60] and the data thus imply a similarly large rate constant for the relevant exciton nonradiative decay process that is eliminated under cathodic bias.

Kinetic Model. The electrobrightening data presented above can be understood using a simple kinetic model. Figure 6 depicts the decay pathways that are active following photoexcitation of ZnSe and Mn^{2+}:ZnSe QDs. In the ZnSe

dx.doi.org/10.1021/ja301102h | J. Am. Chem. Soc. 2012, 134, 6819−6825

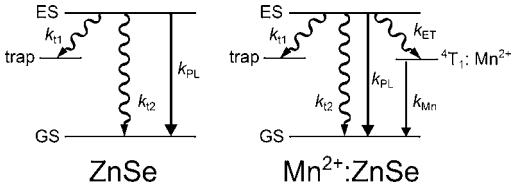

Figure 6. Depiction of the relaxation pathways active following photoexcitation of ZnSe and Mn^{2+}-doped ZnSe QDs. For ZnSe QDs, the photogenerated exciton can decay radiatively (k_{PL}), nonradiatively through an electron trap that is filled at V_{app} (k_{t1}), or nonradiatively through a trap that is unaffected by V_{app} (k_{t2}). For Mn^{2+}-doped ZnSe QDs, the exciton can additionally decay via energy transfer to Mn^{2+} (k_{ET}), which is followed by Mn^{2+} PL (k_{Mn}).

QDs, k_{PL} is the rate constant describing excitonic PL and has a value of 10^8–10^9 s^{-1},[69] k_{t1} describes nonradiative relaxation via the set of electron traps that can be reduced at V_{app}, and k_{t2} describes nonradiative relaxation via traps that are inaccessible at V_{app} (e.g., hole traps, or electron traps at too negative a potential). For the Mn^{2+}:ZnSe QDs, k_{ET} describes exciton-to-Mn^{2+} energy transfer and has a value of $\sim 10^{11}$ s^{-1}.[57−60] k_{Mn} describes decay of the Mn^{2+} $^4T_1$ excited state. For simplicity, nonradiative $^4T_1$ decay is neglected, but the same conclusions are reached if it is treated explicitly. From these schemes, the observation that $I_{EB}/I_0 \approx 40$ for the ZnSe QDs whereas $I_{EB}^{Mn}/I_0^{Mn} \approx 3$ for the Mn^{2+}:ZnSe QDs can be attributed to the introduction of k_{ET} in the latter, as detailed below.

For the ZnSe QDs, the quantum yield for excitonic PL is given by eq 1.

$$\Phi_{PL}^{0} = \frac{k_{PL}}{k_{PL} + k_{t1} + k_{t2}} \tag{1}$$

The Mn^{2+} PL quantum yield in the Mn^{2+}:ZnSe QDs is governed by the energy transfer quantum efficiency (i.e., the branching ratio of the exciton decay), as described by eq 2.

$$\Phi_{Mn}^{0} = \frac{k_{ET}}{k_{ET} + k_{PL} + k_{t1} + k_{t2}} \tag{2}$$

Under a cathodic bias of V_{app}, the accessible traps are reduced and $k_{t1} = 0$. The PL quantum yields for the ZnSe and Mn^{2+}:ZnSe QDs are then described by eqs 3 and 4, respectively.

$$\Phi_{PL}^{EB} = \frac{k_{PL}}{k_{PL} + k_{t2}} \tag{3}$$

$$\Phi_{Mn}^{EB} = \frac{k_{ET}}{k_{ET} + k_{PL} + k_{t2}} \tag{4}$$

Solving eq 1 for k_{t2}, substitution into eq 3, and rearrangement gives eq 5. Similarly, solving eq 2 for k_{t2} and substitution into eq 4 yields eq 6.

$$\frac{k_{t1}}{k_{PL}} = \frac{\Phi_{PL}^{EB} - \Phi_{PL}^{0}}{\Phi_{PL}^{EB} - \Phi_{PL}^{0}} \tag{5}$$

$$\frac{k_{t1}}{k_{ET}} = \frac{\Phi_{Mn}^{EB} - \Phi_{Mn}^{0}}{\Phi_{Mn}^{EB}\Phi_{Mn}^{0}} \tag{6}$$

Equations 5 and 6 illustrate that large electrobrightening occurs when k_{t1} is large relative to the competing rate constant that leads to luminescence (k_{PL} in ZnSe QDs, and k_{ET} in Mn^{2+}:ZnSe QDs). The difference in electrobrightening between ZnSe and Mn^{2+}:ZnSe QDs is thus primarily due to the large difference between k_{ET} and k_{PL} ($\sim 10^{11}$ s^{-1} vs $\sim 10^{9}$ s^{-1}).

Experimentally, the electrobrightening ratios can be measured more reliably than absolute quantum yields. Recasting eq 6 solely in terms of electrobrightening ratios yields eq 7.

$$\frac{k_{t1}}{k_{ET}} = \frac{(I_{EB}/I_0 - 1)(I_{EB}^{Mn}/I_0^{Mn} - 1)}{I_{EB}/I_0 - I_{EB}^{Mn}/I_0^{Mn}} \tag{7}$$

From eq 7, it is evident that in the limit of small Mn^{2+}:ZnSe electrobrightening relative to ZnSe electrobrightening, $k_{t1}/k_{ET} \approx (I_{EB}^{Mn}/I_0^{Mn} - 1)$. Inserting the experimental electrobrightening ratios from Figure 1 into eq 7 yields $k_{t1} \approx 2k_{ET}$, or also $\sim 10^{11}$ s^{-1}. Using the average electrobrightening ratios of all films of each given type yields $k_{t1} \approx 1.5\ k_{ET}$. Although any precise value of this ratio should be interpreted cautiously because of the arbitrariness of the potentials at which electrobrightening was measured, the fact that k_{t1} and k_{ET} are on the same order of magnitude allows the firm conclusions that (i) electron trapping is fast relative to excitonic PL in ZnSe QDs, and (ii) electrobrightening is suppressed by Mn^{2+} doping because energy transfer to Mn^{2+} is comparably fast.

DISCUSSION

The data presented here show that electrobrightening of QD photoluminescence can be large. By changing from CdSe (or other shallow-CB materials) to ZnSe, the CB potential is shifted ~1.0 V more negative, exposing many more electron traps within the semiconductor gap. ZnSe QDs are thus more susceptible to electron trapping than CdSe-based QDs, and hence also show more pronounced and recognizable electrobrightening.

The results here also relate to the proposed "B-type" blinking process deduced from recent single-particle spectroelectrochemical measurements on CdSe/CdS QDs.[51] In these studies, blinking could be suppressed by application of cathodic potentials below the band reduction potential, and hence was associated with surface electron traps. The data here indicate that trapping of photogenerated electrons is extremely fast in ZnSe QDs, and additionally that hot electrons are not integral to this process, as they are in CdSe/CdS QDs.[51] The very negative CB potentials of ZnSe QDs make electron trapping efficient even from the low-energy excitons generated by resonant excitation (λ = 405 nm, see Figure 2). This negative CB potential leads to much more pronounced electrobrightening in ZnSe QDs ($I_{EB}/I_0 \approx 50$) as compared to that estimated from the B-type blinking data of the CdSe/CdS QDs reported in ref 51 ($I_{EB}/I_0 \approx 4$), consistent with a greater density of reducible midgap traps in the ZnSe QDs. The data presented here are thus broadly consistent with the interpretation of electrochemically suppressed blinking proposed in ref 51.

Moreover, our data show that electrobrightening is due to addition of multiple electrons per ZnSe QD; that is, there must be several reducible midgap traps per QD. This observation is important because the reported B-type blinking is a binary phenomenon ("ON" and "OFF" states),[51] and the absence of intermediate PL therefore suggests that even just one active electron trap is sufficient to place a QD in its OFF state. These two considerations may be reconciled if the electron trap population is itself fluxional, for example, through interconversion between different surface ligation modes or related mechanisms of trap spectral diffusion.[70] In this scenario, traps

dx.doi.org/10.1021/ja301102h | J. Am. Chem. Soc. 2012, 134, 6819−6825

would be electrochemically reduced when such fluctuations cause them to appear below V_{app}, and PL of a given QD would become progressively less intermittent as more traps are reduced. It should be noted that precisely the opposite effect (PL quenching) from surface trap filling has also been concluded from spectroelectrochemical studies of CdSe/CdS/ZnS nanocrystals,[46] which obviously cannot be due to the same mechanism as active in the electrobrightening reported here and therefore serves as a reminder of the diversity of QD surface chemistries.

This discussion highlights the fact that little is known about the microscopic identities of surface traps in colloidal QDs. Indeed, the microscopic origins of B-type *blinking* (i.e., the actual cause of the transition between ON and OFF states in the absence of any applied potential) were not explicitly addressed in ref 51. Electron paramagnetic resonance spectroscopy (data not shown) rules out the presence of unpaired electrons at the surfaces of our ZnSe nanocrystals prior to electrochemical reduction, and simple one-electron reduction ("trap filling") of any lattice ion to generate a radical is unlikely. For example, the instability of CB electrons in ZnSe QDs is generally rationalized by comparison of the CB edge potential (~ -1.5 V vs SHE, pH 1) with the two-electron reduction of Zn^{2+} to Zn^0 (~ -0.8 V vs SHE, pH 1) because the one-electron reduction (Zn^{2+} to Zn^+) is unattainable. The relevant surface electrochemistry here likely entails reduction coupled with surface reconstruction involving exogenous ligands. At this time, however, these interesting microscopic issues remain unresolved. Nevertheless, the demonstration here of large electrobrightening in ZnSe QDs reveals a promising and accessible approach to characterization of redox-active surface traps in QDs, with important implications for improving our understanding and control of QD photophysics.

SUMMARY

Large photoluminescence electrobrightening has been observed upon application of a cathodic bias to ZnSe and Mn^{2+}-doped ZnSe QD films in electrochemical cells. The electrobrightening is stable and reversible and can be augmented by photoassisted electrobrightening via a photobias effect. The electrobrightening is attributed to reductive passivation of surface traps at potentials well positive of the ZnSe conduction band potential. The magnitude of the electrobrightening reflects the kinetic competition in the excitonic excited state between electron trapping and processes leading to luminescence. In ZnSe QDs, electron trapping is much faster than radiative electron–hole recombination, and electrobrightening is large. In Mn^{2+}:ZnSe QDs, fast exciton-to-Mn^{2+} energy transfer competes effectively with electron trapping, and consequently the electrobrightening is smaller. These results complement recent observations of reduced blinking in single CdSe-based QDs under cathodic bias[49,51,52] by providing new insight into three aspects of electron-trap-mediated nonradiative decay: (i) electron trapping is fast ($k_{tr} \approx 10^{11}$ s^{-1} at V_{eq}); (ii) multiple electrons per QD are needed to suppress this nonradiative decay channel; and (iii) hot electrons are not integral to the electron-trapping mechanism (even though they may be in specific cases). Overall, the large electrobrightening observed here highlights the attractive possibilities that ZnSe and related semiconductor nanocrystals with very negative conduction-band potentials offer for investigating the trap-related photophysics and spectroelectrochemistry of colloidal QDs. By improving our understanding of how to control QD surface redox chemistries, such investigations may ultimately contribute to improvement of QD-based photovoltaics, light-emitting devices, and bioimaging technologies.

ASSOCIATED CONTENT

Supporting Information

Additional experimental results and data analysis (six figures). This material is available free of charge via the Internet at http://pubs.acs.org.

AUTHOR INFORMATION

Corresponding Author

gamelin@chem.washington.edu

Notes

The authors declare no competing financial interest.

ACKNOWLEDGMENTS

We thank Michael A. White for valuable assistance. Financial support from the US NSF (DMR-0906814) and the University of Washington is also gratefully acknowledged.

REFERENCES

(1) Nirmal, M.; Murray, C. B.; Bawendi, M. G. *Phys. Rev. B: Condens. Matter* **1994**, *50*, 2293–2300.
(2) Kuno, M.; Lee, J. K.; Dabbousi, B. O.; Mikulec, F. V.; Bawendi, M. G. *J. Chem. Phys.* **1997**, *106*, 9869–9882.
(3) Burda, C.; Link, S.; Mohamed, M.; El-Sayed, M. *J. Phys. Chem. B* **2001**, *105*, 12286–12292.
(4) Qu, L.; Peng, X. *J. Am. Chem. Soc.* **2002**, *124*, 2049–2055.
(5) Talapin, D. V.; Rogach, A. L.; Shevchenko, E. V.; Kornowski, A.; Haase, M.; Weller, H. *J. Am. Chem. Soc.* **2002**, *124*, 5782–5790.
(6) Kilina, S.; Ivanov, S.; Tretiak, S. *J. Am. Chem. Soc.* **2009**, *131*, 7717–7726.
(7) Wuister, S. F.; de Mello Donegá, C.; Meijerink, A. *J. Phys. Chem. B* **2004**, *108*, 17393–17397.
(8) Kalyuzhny, G.; Murray, R. W. *J. Phys. Chem. B* **2005**, *109*, 7012–7021.
(9) Hines, M. A.; Guyot-Sionnest, P. *J. Phys. Chem.* **1996**, *100*, 468–471.
(10) Dabbousi, B. O.; Rodriguez-Viejo, J.; Mikulec, F. V.; Heine, J. R.; Mattoussi, H.; Ober, R.; Jensen, K. F.; Bawendi, M. G. *J. Phys. Chem. B* **1997**, *101*, 9463–9475.
(11) van Embden, J.; Jasieniak, J.; Gómez, D. E.; Mulvaney, P.; Giersig, M. *Aust. J. Chem.* **2007**, *60*, 457–471.
(12) Mahler, B.; Spinicelli, P.; Buil, S.; Quelin, X.; Hermier, J.-P.; Dubertret, B. *Nat. Mater.* **2008**, *7*, 659–664.
(13) Chen, Y.; Vela, J.; Htoon, H.; Casson, J. L.; Werder, D. J.; Bussian, D. A.; Klimov, V. I.; Hollingsworth, J. A. *J. Am. Chem. Soc.* **2008**, *130*, 5026–5027.
(14) Reiss, P.; Protière, M.; Li, L. *Small* **2009**, *5*, 154–168.
(15) Wang, X.; Ren, X.; Kahen, K.; Hahn, M. A.; Rajeswaran, M.; Maccagnano-Zacher, S.; Silcox, J.; Cragg, G. E.; Efros, A. L.; Krauss, T. D. *Nature* **2009**, *459*, 686–689.
(16) Nazzal, A. Y.; Wang, X.; Qu, L.; Yu, W.; Wang, Y.; Peng, X.; Xiao, M. *J. Phys. Chem. B* **2004**, *108*, 5507–5515.
(17) Jasieniak, J.; Mulvaney, P. *J. Am. Chem. Soc.* **2007**, *129*, 2841–2848.
(18) Lee, S. F.; Osborne, M. A. *ChemPhysChem* **2009**, *10*, 2174–2191.
(19) Hess, B. C.; Okhrimenko, I. G.; Davis, R. C.; Stevens, B. C.; Schulzke, Q. A.; Wright, K. C.; Bass, C. D.; Evans, C. D.; Summers, S. L. *Phys. Rev. Lett.* **2001**, *86*, 3132.
(20) Manna, L.; Scher, E. C.; Li, L.-S.; Alivisatos, A. P. *J. Am. Chem. Soc.* **2002**, *124*, 7136–7145.
(21) Jones, M.; Nedeljkovic, J.; Ellingson, R. J.; Nozik, A. J.; Rumbles, G. *J. Phys. Chem. B* **2003**, *107*, 11346–11352.

(22) Wang, Y.; Tang, Z.; Correa-Duarte, M. A.; Pastoriza-Santos, I.; Giersig, M.; Kotov, N. A.; Liz-Marzán, L. M. *J. Phys. Chem. B* **2004**, *108*, 15461−15469.
(23) Asami, H.; Abe, Y.; Ohtsu, T.; Kamiya, I.; Hara, M. *J. Phys. Chem. B* **2003**, *107*, 12566−12568.
(24) Cordero, S. R.; Carson, P. J.; Estabrook, R. A.; Strouse, G. F.; Buratto, S. K. *J. Phys. Chem. B* **2000**, *104*, 12137−12142.
(25) Simurda, M.; Nemec, P.; Trojánek, F.; Malý, P. *Thin Solid Films* **2004**, *453*−*454*, 300−303.
(26) Oda, M.; Hasegawa, A.; Iwami, N.; Nishiura, K.; Ando, N.; Nishiyama, A.; Horiuchi, H.; Tani, T. *J. Lumin.* **2007**, *127*, 198−203.
(27) Maenosono, S. *Chem. Phys. Lett.* **2003**, *376*, 666−670.
(28) Kimura, J.; Uematsu, T.; Maenosono, S.; Yamaguchi, Y. *J. Phys. Chem. B* **2004**, *108*, 13258−13264.
(29) Tice, D. B.; Frederick, M. T.; Chang, R. P. H; Weiss, E. A. *J. Phys. Chem. C* **2011**, *115*, 3654−3662.
(30) Duncan, T. V.; Polanco, M. A. M.; Kim, Y.; Park, S.-J. *J. Phys. Chem. C* **2009**, *113*, 7561−7566.
(31) Schafer, S.; Wang, Z.; Kipp, T.; Mews, A. *Phys. Rev. Lett.* **2011**, *107*, 137403.
(32) Hoyer, P.; Weller, H. *J. Phys. Chem.* **1995**, *99*, 14096−14100.
(33) Shim, M.; Guyot-Sionnest, P. *Nature* **2000**, *407*, 981−983.
(34) Shim, M.; Wang, C.; Guyot-Sionnest, P. *J. Phys. Chem. B* **2001**, *105*, 2369−2373.
(35) Wang, C.; Shim, M.; Guyot-Sionnest, P. *Science* **2001**, *291*, 2390−2392.
(36) Haram, S. K.; Quinn, B. M.; Bard, A. J. *J. Am. Chem. Soc.* **2001**, *123*, 8860−8861.
(37) Alperson, B.; Rubinstein, I.; Hodes, G. *Phys. Rev. B: Condens. Matter* **2001**, *63*, 081303.
(38) Wang, C.; Shim, M.; Guyot-Sionnest, P. *Appl. Phys. Lett.* **2002**, *80*, 4−6.
(39) Roest, A. L.; Kelly, J. J.; Vanmaekelbergh, D.; Meulenkamp, E. A. *Phys. Rev. Lett.* **2002**, *89*, 036801.
(40) Wehrenberg, B. L.; Guyot-Sionnest, P. *J. Am. Chem. Soc.* **2003**, *125*, 7806−7807.
(41) Yu, D.; Wang, C.; Guyot-Sionnest, P. *Science* **2003**, *300*, 1277−1280.
(42) Guyot-Sionnest, P.; Wang, C. *J. Phys. Chem. B* **2003**, *107*, 7355−7359.
(43) Wang, C.; Wehrenberg, B. L.; Woo, C. Y.; Guyot-Sionnest, P. *J. Phys. Chem. B* **2004**, *108*, 9027−9031.
(44) Yu, D.; Wehrenberg, B. L.; Jha, P.; Ma, J.; Guyot-Sionnest, P. *J. Appl. Phys.* **2006**, *99*, 104315.
(45) Jha, P. P.; Guyot-Sionnest, P. *J. Phys. Chem. C* **2007**, *111*, 15440−15445.
(46) Gooding, A. K.; Gómez, D. E.; Mulvaney, P. *ACS Nano* **2008**, *2*, 669−676.
(47) Jha, P. P.; Guyot-Sionnest, P. *ACS Nano* **2009**, *3*, 1011−1015.
(48) Araci, Z. O.; Shallcross, C. R.; Armstrong, N. R.; Saavedra, S. S. *J. Phys. Chem. Lett.* **2010**, *1*, 1900−1905.
(49) Jha, P. P.; Guyot-Sionnest, P. *J. Phys. Chem. C* **2010**, *114*, 21138−21141.
(50) White, M. A.; Weaver, A. L.; Beaulac, R.; Gamelin, D. R. *ACS Nano* **2011**, *5*, 4158−4168.
(51) Galland, C.; Ghosh, Y.; Steinbrück, A.; Sykora, M.; Hollingsworth, J. A.; Klimov, V. I.; Htoon, H. *Nature* **2011**, *479*, 203−207.
(52) Qin, W.; Shah, R. A.; Guyot-Sionnest, P. *ACS Nano* **2012**, *6*, 912−918.
(53) Archer, P. I.; Santangelo, S. A.; Gamelin, D. R. *J. Am. Chem. Soc.* **2007**, *129*, 9808−9818.
(54) Li, L. S.; Pradhan, N.; Wang, Y.; Peng, X. *Nano Lett.* **2004**, *4*, 2261−2264.
(55) Norberg, N. S.; Parks, G. L.; Salley, G. M.; Gamelin, D. R. *J. Am. Chem. Soc.* **2006**, *128*, 13195−13203.
(56) Houtepen, A. J.; Vanmaekelbergh, D. *J. Phys. Chem. B* **2005**, *109*, 19634−19642.
(57) Shibata, K.; Nakayama, E.; Souma, I.; Murayama, A.; Oka, Y. *Phys. Status Solidi B* **2002**, *229*, 473−476.
(58) Seufert, J.; Bacher, G.; Scheibner, M.; Forchel, A.; Lee, S.; Dobrowolska, M.; Furdyna, J. K. *Phys. Rev. Lett.* **2002**, *88*, 027402.
(59) Chen, H.-Y.; Chen, T.-Y.; Son, D. H. *J. Phys. Chem. C* **2010**, *114*, 4418−4423.
(60) Vlaskin, V. A.; Janßen, N.; van Rijssel, J.; Beaulac, R.; Gamelin, D. R. *Nano Lett.* **2010**, *10*, 3670−3674.
(61) Beaulac, R.; Ochsenbein, S. T.; Gamelin, D. R. Colloidal Transistion-Metal-Doped Quantum Dots. In *Nanocrystal Quantum Dots*, 2nd ed.; Klimov, V. I., Ed.; Taylor & Francis: London, 2010.
(62) Beaulac, R.; Gamelin, D. R. *Phys. Rev. B* **2010**, *82*, 224401.
(63) Beaulac, R.; Feng, Y.; May, J. W.; Badaeva, E.; Gamelin, D. R.; Li, X. *Phys. Rev. B* **2011**, *84*, 195324.
(64) Madelung, O. *Semiconductors: Data Handbook*, 3rd ed.; Springer: Berlin, 2004.
(65) Wei, S.-H.; Zunger, A. *Appl. Phys. Lett.* **1998**, *72*, 2011−2013.
(66) Vanmaekelbergh, D.; Liljeroth, P. *Chem. Soc. Rev.* **2005**, *34*, 299−312.
(67) Liu, Y.; Gibbs, M.; Puthussery, J.; Gaik, S.; Ihly, R.; Hillhouse, H. W.; Law, M. *Nano Lett.* **2010**, *10*, 1960−1969.
(68) Leatherdale, C. A.; Kagan, C. R.; Morgan, N. Y.; Empedocles, S. A.; Kastner, M. A.; Bawendi, M. G. *Phys. Rev. B: Condens. Matter* **2000**, *62*, 2669−2680.
(69) Balet, L. P.; Ivanov, S. A.; Piryatinski, A.; Achermann, M.; Klimov, V. I. *Nano Lett.* **2004**, *4*, 1485−1488.
(70) Frantsuzov, P.; Kuno, M.; Jankó, B.; Marcus, R. A. *Nat. Phys.* **2008**, *4*, 519−522.